J. Fluid Mech. (2006), *vol.* 557, *pp.* 167–190.
doi:10.1017/S0022112006009670 Printed in the United Kingdom

Boundary-layer analysis for effects of viscosity of the irrotational flow on the flow induced by a rapidly rotating cylinder in a uniform stream

By J. WANG AND D. D. JOSEPH

Department of Aerospace Engineering and Mechanics, University of Minnesota, 110 Union St SE, Minneapolis, MN 55455, USA

(Received 13 March 2005 and in revised form 18 November 2005)

We study the streaming flow past a rapidly rotating circular cylinder. The starting point is the full continuity and momentum equations without any approximations. We assume that the solution is a boundary-layer flow near the cylinder surface with the potential flow outside the boundary layer. The order of magnitude of the terms in the continuity and momentum equations can be estimated inside the boundary layer. When terms of the order of δ/a and higher are dropped, where δ is the boundary-layer thickness and a is the radius of the cylinder, the equations used by M. B. Glauert (*Proc. R. Soc. Lond.* A, vol. 242, 1957, p. 108) are recovered. Glauert's solution ignores the irrotational rotary component of the flow inside the boundary layer, which is consistent with dropping δ/a terms in the governing equations.

We propose a new solution to this problem, in which the velocity field is decomposed into two parts. Outside the boundary layer, the flow is irrotational and can be decomposed into a purely rotary flow and a potential flow past a fixed cylinder. Inside the boundary layer, the velocity is decomposed into an irrotational purely rotary flow and a boundary-layer flow. Inserting this decomposition of the velocity field inside the boundary layer into the governing equations, we obtain a new set of equations for the boundary-layer flow, in which we do not drop the terms of the order of δ/a or higher. The pressure can no longer be assumed to be a constant across the boundary layer, and the continuity of shear stress at the outer edge of the boundary layer is enforced. We solve this new set of equations using Glauert's method, i.e. to expand the solutions as a power series of $\alpha = 2U_0/Q$, where U_0 is the uniform stream velocity and Q is the circulatory velocity at the outer edge of the boundary layer. The pressure from this boundary-layer solution has two parts, an inertial part and a viscous part. The inertial part comes from the inertia terms in the momentum equations and is in agreement with the irrotational pressure; the viscous part comes from the viscous stress terms in the momentum equations and may be viewed as a viscous pressure correction, which contributes to both drag and lift. Our boundary-layer solution is in reasonable to excellent agreement with the numerical simulation in the companion paper by Padrino & Joseph (2006).

1. Introduction

The potential flow over a rotating cylinder in a uniform stream plays an important role in classical airfoil theory in which the flow and airfoil shape is obtained by conformal transformation, and the Kutta condition suppressing separation at the trailing edge is obtained by adjusting the ratio of the rotational speed to the streaming

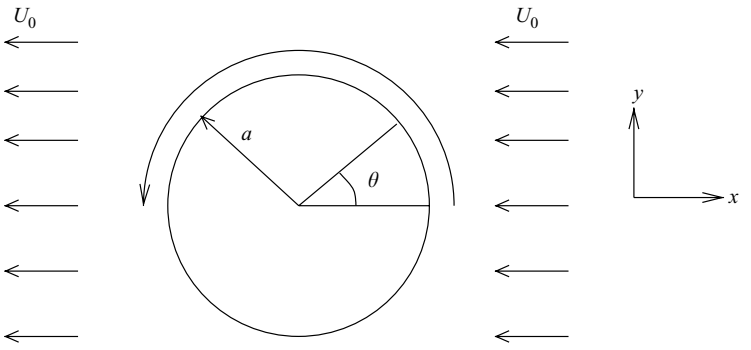

FIGURE 1. The uniform streaming flow past a rotating cylinder.

speed. In our problem, the uniform flow is from right to left and the cylinder rotates counterclockwise (see figure 1). The lift on the cylinder points upward and is defined as positive. The drag on the cylinder is negative if it is in the uniform flow direction; the drag is positive if it is opposite to the uniform flow direction.

The flow pattern depends critically on the ratio between the uniform stream velocity U_0 and the fluid circulatory velocity Q. Potential flow theory shows that when $2U_0/Q < 1$, there is no stagnation point on the cylinder and a region of closed streamlines exists near the cylinder. The fluid circulatory velocity Q is closely related to the peripheral velocity of the cylinder $q = \Omega a$, where Ω is the angular velocity of the cylinder; Q and q are approximately equal for large values of q. Experiments (Prandtl & Tietjens 1931) and simulations (see the companion paper Padrino & Joseph 2006) confirm that separation is largely suppressed and a closed boundary layer around the cylinder may be expected when q is much larger than U_0.

A number of theoretical studies have been dedicated to this problem based on the assumption that the ratio q/U_0 is high, separation is suppressed, and a steady-state solution of the problem exists. Glauert (1957) solved the steady-state two-dimensional boundary-layer equations and obtained the solution in the form of a power series in $\alpha = 2U_0/Q$, which is related to the speed ratio q/U_0 by

$$\alpha \to 2U_0/q = \frac{2}{q/U_0} \quad \text{as} \quad q \to \infty. \tag{1}$$

He carried out the analysis up to and including boundary-layer functions associated with α^4 and obtained

$$\frac{Q}{q} = 1 - 3\left(\frac{U_0}{q}\right)^2 - 3.24\left(\frac{U_0}{q}\right)^4 + \cdots. \tag{2}$$

In his boundary-layer equations, the pressure was assumed to be a constant across the boundary layer; thus the irrotational pressure is the only component in the normal stress acting on the cylinder. The pressure does not contribute to the drag and its contribution to the lift is the same as in the classical aerodynamics equation $L_p = \rho U_0 \Gamma$, where $\Gamma = 2\pi a Q$ is the circulation. The coefficient for the pressure lift is

$$C_{L_p} = \frac{L_p}{\rho U_0^2 a} = 2\pi\frac{Q}{U_0} = 2\pi\frac{q}{U_0}\left[1 - 3\left(\frac{U_0}{q}\right)^2 - 3.24\left(\frac{U_0}{q}\right)^4 + \cdots\right]. \tag{3}$$

The effect of the boundary-layer analysis on the pressure lift is through the value of Q and it should be noted that C_{L_p} is independent of the Reynolds number. Glauert

did not consider the friction drag and lift, but they can be readily obtained from his solution:

$$C_{D_f} = \frac{D_f}{\rho U_0^2 a} = -\frac{2\pi}{\sqrt{Re}}\sqrt{\frac{Q}{U_0}}, \qquad C_{L_f} = \frac{L_f}{\rho U_0^2 a} = \frac{2\pi}{\sqrt{Re}}\sqrt{\frac{Q}{U_0}}, \tag{4}$$

where

$$Re = \frac{2a\rho U_0}{\mu} \tag{5}$$

is the Reynolds number based on the uniform streaming velocity. Glauert computed the torque required to maintain the rotation

$$T = 2\sqrt{2}\pi\rho U_0^{3/2} a^{3/2}\sqrt{\nu}\left[\left(\frac{U_0}{q}\right)^{1/2} - 0.522\left(\frac{U_0}{q}\right)^{5/2} + \cdots\right] \tag{6}$$

and the torque coefficient is

$$C_T = \frac{T}{2\rho U_0^2 a^2} = \frac{2\pi}{\sqrt{Re}}\left[\left(\frac{U_0}{q}\right)^{1/2} - 0.522\left(\frac{U_0}{q}\right)^{5/2} + \cdots\right]. \tag{7}$$

Wood (1957) studied a class of two-dimensional laminar boundary-layer flows with closed streamlines. The velocity at the solid boundary was supposed uniform, and the velocity in the boundary layer was supposed to differ only slightly from that of the boundary. A formal solution of the boundary layer was then derived by expanding the velocity in a power series in a small parameter representative of the small differences of the speed through the boundary layer. He applied the theory to the uniform streaming flow past a rotating cylinder and obtained a circulation which was equivalent to the first two terms of equation (2).

Moore (1957) also considered this problem assuming that the cylinder rotation velocity was much greater than that of the uniform stream. He argued that the effect of the uniform streaming flow could be regarded as a perturbation of the viscous irrotational rotary flow induced by a rotating cylinder and obtained a uniformly valid first approximation to the flow field by solving the streamfunction equation. In the limit of large Reynolds number, Moore also obtained a circulation which was equivalent to the first two terms of equation (2). Moore showed that the drag was small, of the order of $(U_0/q)^3$ and the lift coefficient was

$$C_L = 2\pi\frac{q}{U_0}\left[1 + O\left(\frac{U_0}{q}\right)^2\right], \tag{8}$$

which is comparable to Glauert's pressure lift, (3), but Moore did not give the coefficient of $(U_0/q)^2$. In the limit of large Reynolds number, Moore showed that the torque was

$$T = 4\pi\mu aq\left(1 + \frac{\sqrt{2}}{2}\left(\frac{U_0}{q}\right)^2\sqrt{Re}\right), \tag{9}$$

where the first term on the right-hand side $4\pi\mu aq$ is the torque when there is only viscous irrotational rotary flow, but no streaming flow. The torque coefficient is

$$C_T = \frac{4\pi}{Re}\frac{q}{U_0} + \frac{2\sqrt{2}\pi}{\sqrt{Re}}\frac{U_0}{q}, \tag{10}$$

where the second term on the right-hand side is similar to Glauert's torque coefficient, (7), but the powers of U_0/q are different.

Another problem of the flow past a rotating cylinder is the initial motion after an impulsive start. Ece, Walker & Doligalski (1984) investigated the initial boundary-layer development for an impulsively started translating and rotating cylinder. They solved the time-dependent boundary-layer equations by two methods: an expansion of the solution in a power series in time, and a fully numerical integration of the governing equations. They showed a variety of complex boundary-layer separation flow patterns and demonstrated how separation was affected by increasing rotation rates and how it was ultimately suppressed by the rotation. The temporal development of the drag, lift and torque was presented, but their boundary-layer solution gave no contribution to the pressure drag and lift. They noted that a first-order correction to the vorticity would contribute to the pressure drag and lift comparable to the friction drag and lift; however, the correction was not computed. Their calculation does not last to the time taken for the outer flow to acquire a steady circulation, thus a comparison with the steady boundary-layer solutions, such as Glauert (1957) and Moore (1957), is not possible.

Numerical simulations have been widely used to study the flow past a rotating cylinder. A review of the numerical studies can be found in Padrino & Joseph (2006), who studied flows with high Reynolds numbers ($Re = 200$, 400, 1000) and high speed ratios ($q/U_0 = 3$, 4, 5, 6) using the commercial software Fluent. Their results show that separation is largely suppressed and a steady-state solution can be obtained. Their numerical simulation will serve as the benchmark for the analysis in this work.

We investigate the uniform streaming flow past a rotating cylinder adopting the same assumption as in Glauert (1957), Moore (1957) and Wood (1957), i.e. the cylinder rotation velocity is much greater than that of the uniform stream, separation is suppressed, and a steady-state solution of the problem exists. Our work here is intended to be an improvement of Glauert's boundary-layer solution. The boundary-layer equations used by Glauert can be recovered when terms of the order of δ/a and higher are dropped from the unapproximated continuity and momentum equations. To be consistent, we should have

$$Q\frac{a+\delta}{r} \sim Q \quad \text{for} \quad a \leqslant r \leqslant a+\delta,$$

which means that the irrotational rotary component of the flow inside the boundary layer is ignored. The tangential velocity given by Glauert is

$$u = Q(1 + \alpha f_1' \mathrm{e}^{\mathrm{i}\theta} + \alpha^2[f_2' \mathrm{e}^{2\mathrm{i}\theta} + g_2'] + \cdots), \tag{11}$$

which is a perturbation about a uniform flow, not a perturbation about the viscous irrotational rotary flow. It can be inferred from (11) that the shear stress at the cylinder surface approaches zero when α approaches zero. In other words, Glauert's solution suggests that the shear stress at the cylinder surface approaches zero when the streaming flow is extremely weak compared to the rotation of the cylinder. However, the real limiting value for the shear stress is $-2\mu q/a$. This discrepancy carries on to the computation of the torque. Glauert's torque expression, (6), indicates that the torque is zero when $U_0 = 0$, however, the actual torque to maintain the rotation of the cylinder in a viscous irrotational purely rotary flow is $4\pi\mu aq$, which is also shown in Moore's torque expression, (9).

We propose a new solution to this problem, in which the velocity is decomposed into two parts. Outside the boundary layer, the flow is irrotational and can be decomposed into a viscous irrotational purely rotary flow and a potential flow past a fixed cylinder. Inside the boundary layer, the velocity field is decomposed into a viscous irrotational purely rotary flow and a boundary-layer flow which is expanded as a power series of $\alpha = 2U_0/Q$. This decomposition of the velocity field in the boundary layer is actually a perturbation of the purely rotary flow with α being the perturbation parameter, which is similar to Moore's approach. The difference is that Moore tried to obtain a uniformly valid solution for the flow, whereas we are seeking the solution valid in the boundary layer. Inserting this decomposition of the velocity field inside the boundary layer into the governing equations, we obtain a new set of equations for the boundary-layer flow, in which we do not drop the terms of the order of δ/a or higher. There are significant differences between our new equations and Glauert's boundary-layer equations. In Glauert's study, the pressure is assumed to be a constant across the boundary layer and the momentum equation in the radial direction is not used. The direct result of this approximation by Glauert (and Prandtl), is that the normal stress on a solid is imposed by the irrotational pressure, independent of the Reynolds number. Viscous effects on the normal stress on a solid wall, which always exist at finite-Reynolds number, no matter how large, are not available. In our new equations, the pressure is an unknown and the momentum equation in the radial direction does appear. Because we have an extra unknown, an extra boundary condition is required and we choose to enforce the continuity of the shear stress at the outer edge of the boundary layer. The technique to solve this new set of equations is almost the same as that used by Glauert. The power series expansions are inserted into the new set of equations and the coefficients of different powers of α are compared, then ordinary differential equations for the functions in the power series are obtained and solved. The inertia terms in the momentum equations give rise to the irrotational pressure and the viscous terms lead to a viscous pressure correction, which contributes to both drag and lift.

The idea of a viscous correction of the irrotational pressure has its origin in gas–liquid problems approximated by irrotational flow solutions. One classical example is the drag on a spherical gas bubble of radius a rising in a viscous liquid at high Reynolds number. Levich (1949) obtained the value $12\pi a\mu U$ or equivalently the drag coefficient $48/Re$, by calculating the dissipation of the irrotational flow around the bubble. Moore (1959) calculated the drag directly by integrating the pressure and viscous normal stress of the potential flow and neglecting the viscous shear stress (which physically should be zero), obtaining the value $8\pi a\mu U$. The discrepancy between these two values led G. K. Batchelor, as reported in Moore (1963), to suggest the idea of a pressure correction to the irrotational pressure. It is generally assumed that the pressure correction arises in the boundary layer induced by the discrepancy of the non-zero irrotational shear stress and the zero shear stress at the gas–liquid interface. Moore (1963) performed a boundary-layer analysis and demonstrated that the pressure correction contributes to the drag on the bubble to the same order as the viscous stresses. In his analysis, the lowest-order terms in the momentum equation in the tangential direction involve only the boundary-layer velocity, but not the pressure. Thus, he was able to solve for the boundary-layer velocity first, then insert it into the momentum equation in the radial direction to obtain the pressure correction. The common features of Moore's boundary-layer analysis and our analysis here are that the pressure is not assumed to be a constant across the boundary layer and the momentum equation in the radial direction has to be considered; this is very different

from the classical boundary-layer theory of Prandtl. Moore's pressure correction is readily obtained by setting $y = 0$ in his equation (2.37):

$$p_{\mathrm{v}} = (4/R)(1 - \cos\theta)^2(2 + \cos\theta)/\sin^2\theta, \tag{12}$$

which is singular at the rear stagnation point where $\theta = \pi$ and cannot be used to compute the drag. To obtain the drag coefficient, Moore calculated the momentum defect, and obtained the Levich value $48/Re$ plus contributions of order $Re^{-3/2}$ or lower. The pressure correction which gives rise to the same drag on the bubble as the dissipation calculation has been obtained by Kang & Leal (1988) and Joseph & Wang (2004) by different approaches, neither of which relies on boundary-layer analysis. A boundary-layer analysis which leads to the correct pressure and drag has not been accomplished for the spherical bubble problem. Our analysis here gives rise to a viscous pressure correction in the boundary layer on solids.

One of the key differences between our new boundary-layer analysis and the classical boundary-layer theory of Prandtl is in the calculation of the pressure drag. In the classical boundary-layer approximation, the pressure is constant across the layer and the irrotational pressure of the outer flow is imposed on the surface of the body. This approximation is not good enough for the purpose of the drag calculation and leads to zero pressure drag. Lighthill (1963) remarked, 'Errors, due to neglecting either the pressure gradient across the layer, or the displacement-thickness effect on U, produce a resultant pressure force ("form drag") comparable with the whole viscous force on the body ("skin-friction drag"). Accordingly, such errors cannot be neglected, as often no drag is present from other causes, the pressure forces in pure irrotational flow having zero resultant.' Various techniques were developed to calculate the pressure drag as a patch for Prandtl's theory. Lighthill (1963) described these methods, 'To get round these difficulties, one does not in practice attempt to calculate surface pressure more precisely, but uses a combination of arguments (Chapter X) in which drag is inferred, from conservation of momentum for large masses of fluid, in terms of the state of the boundary layer at the trailing edge.' Schlichting (1960) reviewed methods for the calculation of the profile drag (the sum of the friction drag and the pressure drag) devised by Pretsch (1938) and Squire & Young (1938). These methods are tied in with the boundary-layer calculation and the drag is obtained based on the principle of momentum conservation. Schlichting remarked about these methods, 'However, in order to be in a position to calculate pressure drag it is necessary in each case to make use of certain additional empirical relations.' The method by which we treat the drag is totally different. We solve for the pressure on the body from governing equations. The pressure drag is computed by direct integration of the pressure over the surface of the body, not by arguments of conservation of the momentum.

In our new set of equations for the boundary-layer flow and its boundary conditions, we assume that the boundary-layer thickness δ/a is known, then we can compute the solution. This is different from the problems such as the Blasius' solution, in which the boundary condition at the outer edge of the boundary layer can be stretched to infinity and the solution is obtained without knowledge of the boundary-layer thickness. We prescribe δ/a at different values, compute the solution, then compare them to the results of numerical simulation; the value of δ/a which leads to the best agreement with the simulation results may be viewed as a proper boundary-layer thickness. The boundary-layer thickness determined in this way satisfies approximately $(\delta/a) \propto (1/\sqrt{Re})$ and decreases with increasing q/U_0. Comparison of our solution using the proper δ/a with the simulation results and Glauert's and Moore's solutions shows that our lift and torque are in reasonable to excellent agreement with the simulation results

and the agreement for the drag is less good if the speed ratio q/U_0 is not high enough. It is also demonstrated our solution is indeed an improvement of Glauert's solution.

2. Unapproximated governing equations

Using the polar coordinate system (r, θ), the continuity equation is

$$\frac{\partial v_r}{\partial r} + \frac{v_r}{r} + \frac{1}{r}\frac{\partial v_\theta}{\partial \theta} = 0, \tag{13}$$

and the momentum equations for steady flows are

$$\left(v_r \frac{\partial}{\partial r} + \frac{v_\theta}{r}\frac{\partial}{\partial \theta}\right) v_\theta + \frac{v_r v_\theta}{r} = -\frac{1}{r\rho}\frac{\partial \mathrm{P}}{\partial \theta} + \nu\left(\nabla^2 v_\theta - \frac{v_\theta}{r^2} + \frac{2}{r^2}\frac{\partial v_r}{\partial \theta}\right), \tag{14}$$

$$\left(v_r \frac{\partial}{\partial r} + \frac{v_\theta}{r}\frac{\partial}{\partial \theta}\right) v_r - \frac{v_\theta^2}{r} = -\frac{1}{\rho}\frac{\partial \mathrm{P}}{\partial r} + \nu\left(\nabla^2 v_r - \frac{v_r}{r^2} - \frac{2}{r^2}\frac{\partial v_\theta}{\partial \theta}\right), \tag{15}$$

where

$$\nabla^2 = \frac{\partial^2}{\partial r^2} + \frac{1}{r}\frac{\partial}{\partial r} + \frac{1}{r^2}\frac{\partial^2}{\partial \theta^2}.$$

3. Boundary-layer approximation and Glauert's equations

The flow may be approximated by a boundary layer near the cylinder surface and a potential flow outside. Inside the boundary layer, we have the following estimations

$$v_\theta \sim Q, \quad r \sim a, \quad \frac{\partial}{\partial r} \sim \frac{1}{\delta}, \quad \frac{\partial}{\partial \theta} \sim 1. \tag{16}$$

With these estimates, the magnitude of the terms in (13) can be written as

$$\frac{v_r}{\delta} + \frac{v_r}{a} + \frac{Q}{a} = 0.$$

If we consider v_r/a to be negligible compared to v_r/δ, we have

$$\frac{v_r}{\delta} + \frac{Q}{a} = 0 \;\Rightarrow\; v_r \sim Q\frac{\delta}{a}, \tag{17}$$

and the continuity equation may be written as

$$\frac{\partial v_r}{\partial r} + \frac{1}{r}\frac{\partial v_\theta}{\partial \theta} = 0. \tag{18}$$

We estimate the magnitude of terms in equation (14):

$$\frac{Q^2}{a}\left(1 + 1 + \frac{\delta}{a}\right) = -\frac{1}{r\rho}\frac{\partial \mathrm{P}}{\partial \theta} + \nu\frac{Q}{\delta^2}\left(1 + \frac{\delta}{a} + \frac{\delta^2}{a^2} - \frac{\delta^2}{a^2} + \frac{\delta^3}{a^3}\right). \tag{19}$$

If we drop the terms of the order of δ/a and higher, equation (14) becomes

$$v_r\frac{\partial v_\theta}{\partial r} + \frac{v_\theta}{r}\frac{\partial v_\theta}{\partial \theta} = -\frac{1}{r\rho}\frac{\partial \mathrm{P}}{\partial \theta} + \nu\frac{\partial^2 v_\theta}{\partial r^2}. \tag{20}$$

Now we estimate the magnitude of terms in (15):

$$\frac{Q^2}{a}\left(\frac{\delta}{a} + \frac{\delta}{a} - 1\right) = -\frac{1}{\rho}\frac{\partial \mathrm{P}}{\partial r} + \nu\frac{Q}{\delta^2}\left(\frac{\delta}{a} + \frac{\delta^2}{a^2} + \frac{\delta^3}{a^3} - \frac{\delta^3}{a^3} + \frac{\delta^2}{a^2}\right). \tag{21}$$

Thus, (15) becomes

$$\frac{v_\theta^2}{r} = \frac{1}{\rho}\frac{\partial \mathrm{P}}{\partial r}, \tag{22}$$

which indicates that the change of the pressure across the boundary layer is of the order of δ and the pressure can still be assumed to be constant if δ/a is negligible (Schlichting 1960).

Now if we use x for $r\theta$, y for r, u for v_θ and v for v_r, equations (18) and (20) may be written as

$$\frac{\partial u}{\partial x} + \frac{\partial v}{\partial y} = 0, \tag{23}$$

$$u\frac{\partial u}{\partial x} + v\frac{\partial u}{\partial y} = -\frac{1}{\rho}\frac{\partial \mathrm{P}}{\partial x} + \nu\frac{\partial^2 u}{\partial y^2}, \tag{24}$$

which are the two-dimensional boundary-layer equations used by Glauert (1957). If δ/a terms are dropped, the irrotational rotary component of the velocity inside the boundary layer will be ignored. In reality, the boundary-layer thickness is never zero and is found to be rather large in numerical simulations. Therefore, dropping δ/a terms can cause substantial error.

4. Decomposition of the velocity and pressure field

We propose a new solution, in which the total velocity and pressure are decomposed into two parts

$$v_\theta = u_{p\theta} + u_\theta, \quad v_r = u_r, \quad \mathrm{P} = p_p + p, \tag{25}$$

where

$$u_{p\theta} = Q\frac{a+\delta}{r}, \qquad p_p = p_\infty - \frac{\rho}{2}\frac{(a+\delta)^2}{r^2}Q^2 \tag{26}$$

are the irrotational purely rotary velocity and the pressure induced by rotation. It is noted that $v_\theta = u_{p\theta}$, $v_r = 0$ and $\mathrm{P} = p_p$ is a potential solution and is an exact solution for the unapproximated governing equations and no-slip boundary condition.

Outside the boundary layer, the flow is irrotational and can be decomposed into two potential flows: the irrotational purely rotary flow and the uniform flow past a circle with the radius $a+\delta$. The velocity from the second potential flow is

$$u_\theta = U_0\left[1 + \frac{(a+\delta)^2}{r^2}\right]\sin\theta, \quad u_r = -U_0\left[1 - \frac{(a+\delta)^2}{r^2}\right]\cos\theta. \tag{27}$$

At the outer edge of the boundary layer ($r = a+\delta$), the tangential velocity is

$$v_\theta = 2U_0\sin\theta + Q. \tag{28}$$

The total pressure at $r = a+\delta$ can be obtained from Bernoulli's equation

$$\mathrm{P} = p'_\infty + \tfrac{1}{2}\rho U_0^2(1 - 4\sin^2\theta) - 2\rho U_0 Q\sin\theta - \tfrac{1}{2}\rho Q^2. \tag{29}$$

After subtracting p_p from (29), we obtain the pressure p at $r = a+\delta$

$$p = c + \tfrac{1}{2}\rho U_0^2(1-4\sin^2\theta) - 2\rho U_0 Q\sin\theta = c - \tfrac{1}{2}\rho U_0^2 + \rho U_0^2\cos 2\theta - 2\rho U_0 Q\sin\theta, \tag{30}$$

where c is a certain constant.

Inside the boundary layer, u_θ, u_r and p must be obtained from the governing equations. We insert (25) into the governing equations (13), (14) and (15), subtract

the equations satisfied by $u_{p\theta}$ and p_p, and obtain

$$\frac{\partial u_r}{\partial r} + \frac{u_r}{r} + \frac{1}{r}\frac{\partial u_\theta}{\partial \theta} = 0, \tag{31}$$

$$u_r \frac{\partial}{\partial r}(u_{p\theta} + u_\theta) + \frac{u_{p\theta} + u_\theta}{r}\frac{\partial u_\theta}{\partial \theta} + \frac{u_r(u_{p\theta} + u_\theta)}{r} = -\frac{1}{r\rho}\frac{\partial p}{\partial \theta} + \nu\left(\frac{\partial^2 u_\theta}{\partial r^2} + \frac{1}{r}\frac{\partial u_\theta}{\partial r} + \frac{1}{r^2}\frac{\partial^2 u_\theta}{\partial \theta^2} - \frac{u_\theta}{r^2} + \frac{2}{r^2}\frac{\partial u_r}{\partial \theta}\right), \tag{32}$$

$$u_r \frac{\partial u_r}{\partial r} + \frac{u_{p\theta} + u_\theta}{r}\frac{\partial u_r}{\partial \theta} - \frac{2u_{p\theta}u_\theta + u_\theta^2}{r} = -\frac{1}{\rho}\frac{\partial p}{\partial r} + \nu\left(\frac{\partial^2 u_r}{\partial r^2} + \frac{1}{r}\frac{\partial u_r}{\partial r} + \frac{1}{r^2}\frac{\partial^2 u_r}{\partial \theta^2} - \frac{u_r}{r^2} - \frac{2}{r^2}\frac{\partial u_\theta}{\partial \theta}\right). \tag{33}$$

5. Solution of the boundary-layer flow

We solve equations (31), (32) and (33) for u_θ, u_r and p. Three boundary conditions are imposed on the velocities, u_θ, u_r at $r = a$ and u_θ at $r = a + \delta$; these are the same as in Glauert's analysis. The fourth boundary condition is that the shear stress $\tau_{r\theta}^{BL}$ evaluated using the boundary-layer solution is equal to the shear stress $\tau_{r\theta}^{I}$ evaluated using the outer irrotational flow at $r = a + \delta$. The four boundary conditions are as follows

$$Q\frac{a+\delta}{a} + u_\theta = q \quad \text{at} \quad r = a, \tag{34}$$

$$u_r = 0 \quad \text{at} \quad r = a, \tag{35}$$

$$Q + u_\theta = Q + 2U_0 \sin\theta \quad \text{at} \quad r = a + \delta, \tag{36}$$

$$\tau_{r\theta}^{BL} = \tau_{r\theta}^{I} \quad \text{at} \quad r = a + \delta. \tag{37}$$

Because we are considering a single fluid, the viscosity is the same inside and outside the boundary layer. The continuity of the shear stress (37) is equivalent to continuity of velocity gradients. Glauert's boundary-layer equations can give only solutions with continuous velocity, but our new equations can give solutions with continuous velocity and velocity gradients. We will use complex variables to solve the equations and (36) is written as

$$u_\theta = Q\alpha(-\mathrm{i})\mathrm{e}^{\mathrm{i}\theta} \quad \text{at} \quad r = a + \delta. \tag{38}$$

Note that only the real part of the equation has physical significance.

We follow Glauert and expand the solution as a power series of α. A streamfunction can be written as

$$\psi = Q[\alpha f_1(r)\mathrm{e}^{\mathrm{i}\theta} + \alpha^2(f_2(r)\mathrm{e}^{2\mathrm{i}\theta} + g_2(r))\cdots] \tag{39}$$

and the velocities are

$$u_\theta = \frac{\partial \psi}{\partial r} = Q[\alpha f_1'(r)\mathrm{e}^{\mathrm{i}\theta} + \alpha^2(f_2'(r)\mathrm{e}^{2\mathrm{i}\theta} + g_2'(r))\cdots], \tag{40}$$

$$u_r = -\frac{1}{r}\frac{\partial \psi}{\partial \theta} = -\frac{Q}{r}[\alpha \mathrm{i} f_1(r)\mathrm{e}^{\mathrm{i}\theta} + \alpha^2 2\mathrm{i} f_2(r)\mathrm{e}^{2\mathrm{i}\theta} + \cdots]. \tag{41}$$

The continuity equation (31) is automatically satisfied. The pressure is assumed to be

$$p = p_c + \rho Q^2[\alpha s_1(r)\mathrm{e}^{\mathrm{i}\theta} + \alpha^2(s_2(r)\mathrm{e}^{2\mathrm{i}\theta} + t_2(r))\cdots], \tag{42}$$

where p_c is a constant.

We evaluate $\tau_{r\theta}^I$ using the potential flow (27) and the irrotational rotary flow

$$\tau_{r\theta}^I = -\frac{2\mu Q}{a+\delta} + \mu Q\alpha \frac{2\mathrm{i}}{a+\delta}\mathrm{e}^{\mathrm{i}\theta}. \tag{43}$$

From the boundary-layer solutions, we obtain

$$\tau_{r\theta}^{BL} = -\frac{2\mu Q}{a+\delta} + \mu Q\alpha \left[f_1'' - \frac{f_1'}{a+\delta} + \frac{f_1}{(a+\delta)^2}\right]\mathrm{e}^{\mathrm{i}\theta} + \mu Q\alpha^2 \left[(f_2''\mathrm{e}^{2\mathrm{i}\theta} + g_2'') - \frac{1}{a+\delta}(f_2'\mathrm{e}^{2\mathrm{i}\theta} + g_2') + \frac{4}{(a+\delta)^2} f_2\mathrm{e}^{2\mathrm{i}\theta}\right] + \cdots. \tag{44}$$

Comparing the terms in (43) and (44) linear in α, we obtain

$$\frac{2\mathrm{i}}{a+\delta} = f_1'' - \frac{f_1'}{a+\delta} + \frac{f_1}{(a+\delta)^2} \quad \text{at} \quad r = a+\delta. \tag{45}$$

Consideration of the terms quadratic in α gives

$$f_2'' - \frac{1}{a+\delta} f_2' + \frac{4}{(a+\delta)^2} f_2 = 0, \qquad g_2'' - \frac{1}{a+\delta} g_2' = 0 \quad \text{at} \quad r = a+\delta. \tag{46}$$

In this study, one of the major objects is to determine the relation between the cylinder velocity q and the fluid circulatory velocity Q. In the expansion of the boundary-layer velocities (40) and (41), Q is used as the fundamental parameter rather than q. As noted by Glauert, this approach is convenient for the study of the boundary-layer equations because the velocity at the outer edge of the boundary layer is completely specified. Though Q is an unknown quantity and q is prescribed, the relationship between q and Q can be established via (34), giving Q in terms of q. We also note that the boundary-layer thickness δ appears in the boundary conditions and it must be prescribed to obtain the solution. It can be expected that the boundary-layer thickness is a function of θ, but we are not able to determine the shape of the boundary layer. We will assume that δ is a constant for given Re and q/U_0; it may be viewed as the average boundary-layer thickness. The choice of δ has significant effects on the solution and will be discussed later.

We insert (40), (41) and (42) into (32) and (33) and compare the coefficients of different powers of α, to obtain ordinary differential equations for $f_1(r)$, $f_2(r)$, $g_2(r)\ldots$. The terms linear in α in (32) and (33) satisfy, respectively,

$$\frac{Q(a+\delta)}{r} f_1' = -Qs_1 + \frac{\nu}{\mathrm{i}}\left(rf_1''' + f_1'' - \frac{2f_1'}{r} + \frac{2f_1}{r^2}\right), \tag{47}$$

$$\frac{Q(a+\delta)}{r^3} f_1 - \frac{2Q(a+\delta)}{r^2} f_1' = -Qs_1' + \frac{\nu}{\mathrm{i}}\left(\frac{f_1''}{r} + \frac{1}{r^2} f_1' - \frac{1}{r^3} f_1\right). \tag{48}$$

After eliminating s_1 from (47) and (48), we obtain a fourth-order ordinary differential equation for f_1

$$\frac{Q(a+\delta)}{\nu}\mathrm{i}\left(\frac{f_1''}{r} + \frac{f_1'}{r^2} - \frac{f_1}{r^3}\right) = rf_1'''' + 2f_1''' - \frac{3}{r} f_1'' + \frac{3}{r^2} f_1' - \frac{3}{r^3} f_1, \tag{49}$$

where $Q(a+\delta)/\nu$ is a Reynolds number and we write

$$k = \frac{\nu}{Q(a+\delta)}. \tag{50}$$

The solution of (49) is

$$f_1(r) = \frac{c_1}{r} + c_2 r^{2-\beta} + c_3 r^{2+\beta} + c_4 r, \tag{51}$$

where c_1, c_2, c_3 and c_4 are constants to be determined by boundary conditions and

$$\beta = \sqrt{1 + \frac{\mathrm{i}}{k}}. \tag{52}$$

Three boundary conditions for f_1 are obtained from (34), (35) and (38)

$$f_1(a) = 0, \quad f_1'(a) = 0, \quad f_1'(a+\delta) = -\mathrm{i}. \tag{53}$$

The fourth condition is the continuity of the shear stress (45), which can be written as

$$\frac{\mathrm{i}}{a+\delta} = f_1'' + \frac{f_1}{(a+\delta)^2} \quad \text{at} \quad r = a+\delta. \tag{54}$$

With these four boundary conditions, we can determine c_1, c_2, c_3 and c_4 and the function f_1. The expression for f_1 is long and will not be shown here.

After we obtain $f_1(r)$, we can compute $s_1(r)$ using equation (47)

$$s_1 = -\frac{a+\delta}{r} f_1' + \frac{\nu}{Q}\zeta, \tag{55}$$

where

$$\zeta = \frac{1}{\mathrm{i}}\left(r f_1''' + f_1'' - \frac{2}{r} f_1' + \frac{2}{r^2} f_1\right). \tag{56}$$

The two parts of s_1, $(-((a+\delta)/r)\, f_1')$ and $(\nu/Q)\zeta$ come from the inertia term and viscous stress term in the momentum equation, respectively.

Next we carry out the calculation for terms quadratic in α. As pointed out by Glauert, care should be taken when computing the product of two complex numbers A and B,

$$\mathrm{Re}(A)\mathrm{Re}(B) = \mathrm{Re}(A(B+\overline{B})/2), \tag{57}$$

where the overbar denotes a complex conjugate. We collect terms quadratic in α from (32) and they can be divided into two groups, terms proportional to $\mathrm{e}^{2\mathrm{i}\theta}$ and terms independent of θ. The two groups of terms satisfy the following equations, respectively

$$\frac{1}{r}\frac{Q\mathrm{i}}{\nu}\left(\tfrac{1}{2} f_1'^2 - \tfrac{1}{2} f_1 f_1'' - \frac{1}{2r} f_1 f_1' + \frac{2(a+\delta)}{r} f_2'\right) = -\frac{Q\mathrm{i}}{\nu}\frac{2 s_2}{r} + \left(f_2''' + \frac{f_2''}{r} - \frac{5 f_2'}{r^2} + \frac{8 f_2}{r^3}\right), \tag{58}$$

$$-\frac{1}{2r}\frac{Q\mathrm{i}}{\nu}\left(f_1\overline{f_1''} + f_1'\overline{f_1'} + \frac{f_1}{r}\overline{f_1'}\right) = g_2''' + \frac{g_2''}{r} - \frac{g_2'}{r^2}. \tag{59}$$

Consideration of terms in (33) quadratic in α also yields two equations

$$\frac{1}{r}\frac{Q\mathrm{i}}{\nu}\left(\frac{1}{2r^2} f_1^2 - \tfrac{1}{2} f_1'^2 + \frac{4(a+\delta)}{r^2} f_2 - \frac{2(a+\delta)}{r} f_2'\right) = -\frac{Q\mathrm{i}}{\nu} s_2' - \left(\frac{8}{r^3} f_2 - \frac{2}{r^2} f_2' - \frac{2}{r} f_2''\right), \tag{60}$$

$$\frac{1}{r}\left(\frac{1}{2r} f_1\overline{f_1'} + \frac{1}{2r} f_1'\overline{f_1} - \frac{1}{2r^2} f_1\overline{f_1} - \tfrac{1}{2} f_1'\overline{f_1'} - \frac{2(a+\delta)}{r} g_2'\right) = -t_2'. \tag{61}$$

We can first solve $g_2(r)$ from (59), then eliminate $s_2(r)$ from (58) and (60) and solve for $f_2(r)$, finally obtain $t_2(r)$ from (61).

Equation (59) is a third-order ordinary differential equation for g_2. We prescribe the streamfunction at $r=a$ to be zero, which gives the condition

$$g_2(a)=0. \tag{62}$$

The boundary condition (38) leads to

$$g_2'(a+\delta)=0. \tag{63}$$

The continuity of the shear stress (46) leads to

$$g_2''(a+\delta)=0. \tag{64}$$

No condition can be applied to $g_2'(r=a)$, because it is only known that the surface velocity is independent of θ. Thus we have three boundary conditions (62), (63) and (64) for the third-order ordinary differential equation (59). A closed-form solution for $g_2(r)$ can be obtained, but it is long and tedious and will not be shown here.

We eliminate s_2 from (58) and (60) and obtain a fourth-order ordinary differential equation for f_2

$$\begin{aligned}\frac{Q\mathrm{i}}{\nu}\left(-\tfrac{1}{2}f_1f_1'''+\tfrac{1}{2}f_1'f_1''-\frac{1}{2r}f_1f_1''+\frac{1}{2r}f_1'f_1'+\frac{1}{2r^2}f_1f_1'-\frac{1}{r^3}f_1^2\right)\\ =rf_2''''+2f_2'''-\frac{9}{r}f_2''+\frac{9}{r^2}f_2'-\frac{Q(a+\delta)\mathrm{i}}{\nu}\left(\frac{2}{r}f_2''+\frac{2}{r^2}f_2'-\frac{8}{r^3}f_2\right).\end{aligned} \tag{65}$$

Three boundary conditions for $f_2(r)$ are obtained from (34), (35) and (38)

$$f_2(a)=0,\quad f_2'(a)=0,\quad f_2'(a+\delta)=0, \tag{66}$$

and the fourth condition comes from the continuity of the shear stress (46)

$$f_2''+\frac{4}{(a+\delta)^2}f_2=0\quad\text{at}\quad r=a+\delta. \tag{67}$$

Equation (65) and the boundary conditions are solved by numerical integration.

After $f_2(r)$ is obtained, we compute $s_2(r)$ using (58)

$$s_2=-\tfrac{1}{4}f_1'^2+\tfrac{1}{4}f_1f_1''+\frac{1}{4r}f_1f_1'-\frac{a+\delta}{r}f_2'+\frac{\nu}{2Q}\xi, \tag{68}$$

where

$$\xi=\frac{1}{\mathrm{i}}\left(rf_2'''+f_2''-\frac{5}{r}f_2'+\frac{8}{r^2}f_2\right). \tag{69}$$

The function s_2 can be divided into two parts, the term $(\nu/2Q)\xi$ comes from the viscous stress and other terms in s_2 come from the inertia terms in the momentum equation.

The last step in the calculation of terms quadratic in α is to integrate (61) to obtain $t_2(r)$. There will be an undetermined constant in the process of integration, which can be absorbed into the pressure constant p_c.

With the functions s_1 and s_2, we can write the pressure as

$$\begin{aligned} p &= p_c + \rho Q^2 \alpha s_1 \mathrm{e}^{\mathrm{i}\theta} + \rho Q^2 \alpha^2 \left(s_2 \mathrm{e}^{2\mathrm{i}\theta} + t_2\right) + O(\alpha^3) \\ &= p_c + 2\rho U_0 Q \left(-\frac{a+\delta}{r} f_1' + \frac{\nu}{Q}\zeta\right) \mathrm{e}^{\mathrm{i}\theta} \\ &\quad + 4\rho U_0^2 \left[\left(-\frac{1}{4} f_1'^2 + \frac{1}{4} f_1 f_1'' + \frac{1}{4r} f_1 f_1' - \frac{a+\delta}{r} f_2' + \frac{\nu}{2Q}\xi\right) \mathrm{e}^{2\mathrm{i}\theta} + t_2\right] + O(\alpha^3). \end{aligned} \tag{70}$$

The pressure at the outer edge of the boundary layer is of interest, because it can be compared to the irrotational pressure (30) at $r = a+\delta$ and the difference between them gives the pressure correction. From (53), $f_1'(a+\delta) = -\mathrm{i}$ and from (66), $f_2'(a+\delta) = 0$, the pressure at $r = a+\delta$ is

$$p = p_c + 2\rho U_0 Q \left(\mathrm{i} + \frac{\nu}{Q}\zeta\right) \mathrm{e}^{\mathrm{i}\theta} + \rho U_0^2 \left[\left(1 + f_1 f_1'' - \frac{\mathrm{i}}{a+\delta} f_1 + \frac{2\nu}{Q}\xi\right) \mathrm{e}^{2\mathrm{i}\theta} + 4t_2\right] + O(\alpha^3). \tag{71}$$

The real part of the above equation is

$$\begin{aligned} p &= \mathrm{Re}(p_c) + 4\rho U_0^2 \mathrm{Re}(t_2) - 2\rho U_0 Q \sin\theta + \rho U_0^2 \cos 2\theta + \rho U_0^2 \mathrm{Re}\left[\left(f_1 f_1'' - \frac{\mathrm{i}}{a+\delta} f_1\right) \mathrm{e}^{2\mathrm{i}\theta}\right] \\ &\quad + 2\mu U_0 \left[\mathrm{Re}(\zeta)\cos\theta - \mathrm{Im}(\zeta)\sin\theta\right] + 2\mu \frac{U_0^2}{Q} \left[\mathrm{Re}(\xi)\cos 2\theta - \mathrm{Im}(\xi)\sin 2\theta\right] + O(\alpha^3). \end{aligned} \tag{72}$$

Because the radial component u_r of the velocity is small in the boundary layer, we may neglect f_1, then compare (72) to the irrotational pressure (30). The terms $-2\rho U_0 Q \sin\theta$ and $\rho U_0^2 \cos 2\theta$ are the same in the two pressure expressions, and the terms proportional to μ in (72) are the extra pressure arising in the boundary layer. This comparison demonstrates that the inertia terms in the momentum equations give rise to the irrotational pressure and the viscous stress terms give rise to a viscous pressure correction. In general, the pressure correction can be expanded as a Fourier series

$$p_{\mathrm{v}} = \sum_{m=0}^{\infty} \left[h_m(r)\cos m\theta + j_m(r)\sin m\theta\right].$$

Here we determine the coefficients of $\sin\theta$, $\cos\theta$, $\sin 2\theta$ and $\cos 2\theta$ up to $O(\alpha^2)$ terms. These coefficients may be modified and more coefficients in the Fourier series can be obtained if calculations for $O(\alpha^3)$ terms are carried out. The $\cos\theta$ and $\sin\theta$ terms in the pressure correction contribute to the drag and lift, respectively.

Up to this point, our solutions are in terms of the fluid circulatory velocity Q. We shall solve for Q in terms of the prescribed quantities using an iterative method. There are two prescribed dimensionless parameters in this problem, the Reynolds number Re and the speed ratio q/U_0. Our first guess of Q comes from the irrotational purely rotary flow

$$Q^{(1)} = q\frac{a}{a+\delta} \;\Rightarrow\; \frac{Q^{(1)}}{q} = \frac{1}{1+\delta/a},$$

where the superscript (1) indicates the value for Q in the first iteration. Using $Q^{(1)}/q$, the value of k is computed in equation (50) and $f_1(r)$ is subsequently obtained. Then

we solve for $g_2(r)$ from equation (59) and obtain g_2'. The velocity u_θ at $r=a$ is then

$$u_\theta = Q^{(1)}\alpha^2 \mathrm{Re}[g_2'(r=a,\, Q^{(1)}/q)] + O(\alpha^3). \tag{73}$$

Inserting (73) into (34), we obtain

$$\frac{Q^{(2)}}{q}\frac{a+\delta}{a} + 4\frac{U_0^2}{q^2}\frac{q}{Q^{(1)}}\mathrm{Re}\left[g_2'\left(r=a,\, Q^{(1)}/q\right)\right] = 1, \tag{74}$$

from which we can solve for $Q^{(2)}$, which is the value for Q in the second iteration. We repeat the calculation using $Q^{(2)}$ to obtain the value for Q in the next iteration, until the value of Q converges.

The functions s_1, f_2, s_2 and t_2 are computed following the procedure described above and the solution of the boundary-layer equations are determined up to $O(\alpha^2)$. We can compute the pressure and shear stress at the cylinder surface and integrate to obtain the drag, lift and torque. The drag and lift by the pressure are

$$D_p = \int_A \boldsymbol{e}_x \cdot (-P\mathbf{1}) \cdot \boldsymbol{e}_r \,\mathrm{d}A = \int_0^{2\pi} (-P)\cos\theta\, a\,\mathrm{d}\theta = -\rho Q^2 \alpha\, \mathrm{Re}(s_1)\pi a, \tag{75}$$

$$L_p = \int_A \boldsymbol{e}_y \cdot (-P\mathbf{1}) \cdot \boldsymbol{e}_r \,\mathrm{d}A = \int_0^{2\pi} (-P)\sin\theta\, a\,\mathrm{d}\theta = \rho Q^2 \alpha\, \mathrm{Im}(s_1)\pi a. \tag{76}$$

The friction drag and lift by the shear stress are

$$D_f = \int_A \boldsymbol{e}_x \cdot (\tau_{\theta r}\boldsymbol{e}_\theta\boldsymbol{e}_r) \cdot \boldsymbol{e}_r \,\mathrm{d}A = \int_0^{2\pi} \tau_{\theta r}(-\sin\theta)\, a\,\mathrm{d}\theta = \mu Q\alpha\, \mathrm{Im}(f_1'')\pi a, \tag{77}$$

$$L_f = \int_A \boldsymbol{e}_y \cdot (\tau_{\theta r}\boldsymbol{e}_\theta\boldsymbol{e}_r) \cdot \boldsymbol{e}_r \,\mathrm{d}A = \int_0^{2\pi} \tau_{\theta r}\cos\theta\, a\,\mathrm{d}\theta = \mu Q\alpha\, \mathrm{Re}(f_1'')\pi a. \tag{78}$$

We call the readers' attention to the fact that in our problem, the drag on the cylinder is negative if it is in the uniform flow direction; the drag is positive if it is opposite to the uniform flow direction (see figure 1). The drag and lift coefficients are defined as

$$C_{D_p} = \frac{D_p}{\rho U_0^2 a}, \qquad C_{D_f} = \frac{D_f}{\rho U_0^2 a}, \qquad C_D = \frac{D_p + D_f}{\rho U_0^2 a}, \tag{79}$$

$$C_{L_p} = \frac{L_p}{\rho U_0^2 a}, \qquad C_{L_f} = \frac{L_f}{\rho U_0^2 a}, \qquad C_L = \frac{L_p + L_f}{\rho U_0^2 a}. \tag{80}$$

The torque is

$$T = -a^2 \int_0^{2\pi} \tau_{\theta r}\,\mathrm{d}\theta = 2\pi\mu a^2 \left(2Q\frac{a+\delta}{a^2} - Q\alpha^2 g_2'' + \frac{Q\alpha^2}{a} g_2'\right), \tag{81}$$

with the dimensionless torque defined as

$$C_T = \frac{T}{2\rho U_0^2 a^2}. \tag{82}$$

In tables 1–6, we give the drag, lift and torque computed from our boundary-layer solutions and compare them to the results of numerical simulation from Padrino & Joseph (2006) for six cases, $(Re,\, q/U_0) = (200,\, 4)$, (200, 5), (400, 4), (400, 5), (400, 6) and (1000, 3). The boundary-layer thickness δ/a is prescribed at different values; when the value of δ/a falls into a certain range (highlighted in bold type in tables 1–6), our analysis gives rise to lift and torque in good agreement with the simulation results. The agreement for the drag is less good, which is partly due to the fact that the absolute value of the drag is small and the relative error is apparent. Nevertheless,

δ/a	q/Q	C_{D_p}	C_{D_f}	C_D	C_{L_p}	C_{L_f}	C_L	C_T
0.1	1.114	−13.551	−1.388	−14.939	21.563	0.414	21.978	0.277
0.15	1.221	−5.090	−1.010	−6.100	21.303	0.587	21.891	0.328
0.2	1.409	−1.669	−0.848	−2.517	20.153	0.697	20.850	0.400
0.23	1.580	−0.620	−0.788	−1.408	18.938	0.725	19.663	0.446
0.24	**1.649**	**−0.381**	**−0.770**	**−1.152**	**18.444**	**0.729**	**19.173**	**0.461**
0.25	**1.726**	**−0.188**	**−0.754**	**−0.942**	**17.907**	**0.729**	**18.636**	**0.476**
0.26	**1.812**	**−0.0351**	**−0.737**	**−0.772**	**17.329**	**0.727**	**18.056**	**0.490**
0.27	1.907	0.0815	−0.721	−0.639	16.710	0.722	17.432	0.504
0.28	2.012	0.166	−0.704	−0.538	16.055	0.714	16.769	0.517
Simulation results		0.728	−0.604	0.124	16.961	0.621	17.582	0.453

TABLE 1. The comparison of the coefficients for the drag, lift and torque with the simulation results for $Re = 200$ and $q/U_0 = 4$. The lift and torque computed using $\delta/a = 0.24$, 0.25 or 0.26 are in reasonable agreement with the results of numerical simulation. The drag, especially the drag due to the pressure, does not agree well with the simulation results. When $\delta/a = 0.28$, the value of q/Q is such that $\alpha = 2U_0/Q > 1$, which makes the power series expansions of the solutions in terms of α divergent. The calculation can be performed, but cannot be expected to converge to the true result.

δ/a	q/Q	C_{D_p}	C_{D_f}	C_D	C_{L_p}	C_{L_f}	C_L	C_T
0.1	1.114	−13.061	−1.400	−14.461	27.039	0.517	27.556	0.346
0.15	1.218	−4.157	−1.044	−5.201	27.007	0.730	27.736	0.407
0.19	1.350	−0.988	−0.928	−1.916	26.414	0.845	27.259	0.473
0.2	**1.392**	**−0.468**	**−0.909**	**−1.377**	**26.164**	**0.866**	**27.029**	**0.490**
0.21	**1.437**	**−0.0296**	**−0.893**	**−0.922**	**25.870**	**0.883**	**26.752**	**0.507**
0.22	**1.486**	**0.337**	**−0.878**	**−0.541**	**25.531**	**0.896**	**26.428**	**0.524**
0.25	1.659	1.089	−0.841	0.248	24.243	0.920	25.163	0.574
0.3	2.072	1.531	−0.779	0.752	21.111	0.903	22.014	0.650
0.35	2.804	1.318	−0.690	0.628	16.512	0.813	17.324	0.714
Simulation results		0.824	−0.835	−0.0107	26.183	0.846	27.029	0.514

TABLE 2. The comparison of the coefficients for the drag, lift and torque with the simulation results for $Re = 200$ and $q/U_0 = 5$. The lift and torque computed using $\delta/a = 0.2$, 0.21 or 0.22 are in excellent agreement with the results of numerical simulation. The agreement of drag, especially the drag due to the pressure, is not good. When $\delta/a = 0.35$, $\alpha = 2U_0/Q > 1$, and the power series expansions of the solutions in terms of α are divergent.

δ/a	q/Q	C_{D_p}	C_{D_f}	C_D	C_{L_p}	C_{L_f}	C_L	C_T
0.1	1.155	−5.629	−0.724	−6.352	21.104	0.396	21.499	0.173
0.13	1.277	−2.249	−0.610	−2.859	20.292	0.470	20.762	0.215
0.15	1.398	−1.008	−0.565	−1.572	19.357	0.498	19.855	0.246
0.16	1.472	−0.582	−0.547	−1.129	18.766	0.506	19.272	0.261
0.17	**1.558**	**−0.258**	**−0.530**	**−0.788**	**18.094**	**0.509**	**18.603**	**0.276**
0.18	**1.657**	**−0.0178**	**−0.514**	**−0.532**	**17.343**	**0.509**	**17.852**	**0.291**
0.2	1.906	0.260	−0.483	−0.223	15.613	0.497	16.110	0.318
0.23	2.466	0.316	−0.432	−0.116	12.551	0.453	13.004	0.352
Simulation results		0.534	−0.451	−0.0836	17.609	0.447	18.057	0.275

TABLE 3. The comparison of the coefficients for the drag, lift and torque with the simulation results for $Re = 400$ and $q/U_0 = 4$. The lift and torque computed using $\delta/a = 0.17$ or 0.18 are in excellent agreement with the results of numerical simulation. The agreement of drag, especially the drag due to the pressure, is not good. When $\delta/a = 0.23$, $\alpha = 2U_0/Q > 1$, and the power series expansions of the solutions in terms of α are divergent.

δ/a	q/Q	C_{D_p}	C_{D_f}	C_D	C_{L_p}	C_{L_f}	C_L	C_T
0.1	1.153	−4.803	−0.746	−5.550	26.670	0.491	27.187	0.215
0.13	1.266	−1.190	−0.650	−1.840	26.140	0.582	26.722	0.263
0.14	**1.315**	**−0.457**	**−0.631**	**−1.089**	**25.816**	**0.602**	**26.419**	**0.280**
0.15	**1.370**	**0.112**	**−0.617**	**−0.504**	**25.420**	**0.618**	**26.038**	**0.297**
0.16	**1.431**	**0.548**	**−0.604**	**−0.056**	**24.952**	**0.630**	**25.582**	**0.314**
0.2	1.750	1.386	−0.565	0.821	22.366	0.641	23.007	0.374
0.25	2.502	1.313	−0.493	0.820	16.923	0.577	17.500	0.440
Simulation results		0.591	−0.601	−0.010	26.415	0.597	27.011	0.297

TABLE 4. The comparison of the coefficients for the drag, lift and torque with the simulation results for $Re = 400$ and $q/U_0 = 5$. The lift and torque computed using $\delta/a = 0.14$ or 0.15, and the drag computed using $\delta/a = 0.16$ are in good agreement with the results of numerical simulation. When $\delta/a = 0.25$, $\alpha = 2U_0/Q > 1$, and the power series expansions of the solutions in terms of α divergent.

δ/a	q/Q	C_{D_p}	C_{D_f}	C_D	C_{L_p}	C_{L_f}	C_L	C_T
0.1	1.151	−3.860	−0.773	−4.633	32.48	0.585	33.06	0.256
0.12	1.216	−1.031	−0.714	−1.744	32.48	0.660	33.14	0.290
0.13	1.254	−0.0650	−0.697	−0.762	32.42	0.690	33.11	0.308
0.135	**1.274**	**0.331**	**−0.691**	**−0.361**	**32.37**	**0.703**	**33.07**	**0.316**
0.14	**1.296**	**0.676**	**−0.686**	**−0.0105**	**32.31**	**0.714**	**33.03**	**0.325**
0.145	**1.317**	**0.975**	**−0.682**	**0.293**	**32.24**	**0.725**	**32.97**	**0.333**
0.15	1.340	1.233	−0.679	0.554	32.16	0.734	32.90	0.342
0.2	1.577	2.318	−0.678	1.641	31.31	0.788	32.10	0.408
Simulation results		0.668	−0.681	−0.0136	33.09	0.682	33.77	0.316

TABLE 5. The comparison of the coefficients for the drag, lift and torque with the simulation results for $Re = 400$ and $q/U_0 = 6$. The drag, lift and torque computed using $\delta/a = 0.14$ are in excellent agreement with the results of numerical simulation. The calculation is reasonably accurate in the range $0.135 \leqslant \delta/a \leqslant 0.145$.

δ/a	q/Q	C_{D_p}	C_{D_f}	C_D	C_{L_p}	C_{L_f}	C_L	C_T
0.08	1.217	−3.185	−0.362	−3.547	14.72	0.220	14.94	0.0801
0.1	1.418	−1.509	−0.310	−1.819	13.20	0.237	13.44	0.106
0.12	**1.755**	**−0.755**	**−0.273**	**−1.028**	**11.08**	**0.232**	**11.31**	**0.130**
Simulation results		0.213	−0.197	0.0155	10.41	0.192	10.60	0.118

TABLE 6. The comparison of the coefficients for the drag, lift and torque with the simulation results for $Re = 1000$ and $q/U_0 = 3$. The lift and torque computed using $\delta/a = 0.1$ or 0.12 are close to the results of numerical simulation. However, it should be noted that $\alpha = 1.17 > 1$ when $\delta/a = 0.12$ and the power series expansions of the solutions in terms of α divergent. This is caused by the relatively low value of the speed ratio $q/U_0 = 3$. If Glauert's solution is used for this case, $\alpha = 1.064$ and Glauert's solution also diverges.

good agreement for the drag is obtained in the cases $(Re, q/U_0) = (400, 5)$ and (400, 6), which are the ones with relatively large values of Re and q/U_0 in the six cases. This indicates that the agreement for the drag becomes better as the prescribed parameters move toward the range in which the theory is supposed to work better. Our solution for $(Re, q/U_0) = (400, 6)$ using $\delta/a = 0.14$ (see table 5) is in excellent agreement with the results of numerical simulation.

We highlight the range of δ/a in which the lift and torque are in good agreement with the simulation results in tables 1–6. We choose one value from this range (typically the median) as a proper boundary-layer thickness: $\delta/a = 0.25$, 0.21, 0.17, 0.15, 0.14 and 0.12 for $(Re,\ q/U_0) = (200,\ 4)$, (200, 5), (400, 4), (400, 5), (400, 6) and (1000, 3), respectively. As expected, the boundary-layer thickness decreases with increasing Reynolds number and the relation $(\delta/a) \propto (1/\sqrt{Re})$ seems to hold when q/U_0 is fixed. The boundary-layer thickness also decreases with increasing q/U_0, because the rotary flow suppresses the boundary layer induced by the streaming flow.

The choice of δ/a is vital in our calculation. If δ/a is much smaller than the proper boundary-layer thickness, the flow there cannot match the potential flow outside, which breaks the assumptions of our calculation. If δ/a is much larger than the proper boundary-layer thickness, the value of Q is small and $\alpha = 2U_0/Q$ could be close to 1 or even larger than 1, which makes the power series expansion of the solutions in terms of α slow to converge or even divergent. On the other hand, there are a range of δ/a values which can lead to lift and torque in good agreement with simulation results, because there is no clear-cut boundary-layer edge physically. The calculation is reasonably accurate when δ/a falls in this range.

We compare the drag, lift and torque given by our solution using the proper δ/a, by Glauert's solution, by Moore's solution and by the numerical simulation in table 7. Equations (3), (4) and (7) are used to compute the lift, drag and torque coefficients given by Glauert's solution. Equation (10) is used to compute the torque given by Moore's solution; the drag and lift are not computed since Moore did not give the necessary coefficients. The comparison demonstrates that Moore's torque is relatively close to the simulation results, and Glauert's solution gives reasonable approximations for the friction drag and lift, but poor approximation for the torque. It also confirms that our solution is indeed an improvement of Glauert's solution, especially in the category of torque.

A key feature of this boundary-layer analysis is that the variation of the pressure across the boundary layer is obtained. We integrate the drag and lift components of the pressure over circles concentric with the cylinder but with different radii, then C_{D_p} and C_{L_p} become functions of r. We compare these functions computed from our boundary-layer analysis and from numerical simulation by Padrino & Joseph (2006) in figures 2 and 3.

The functions $C_{D_p}(r)$ for three cases, $Re = 400$ and $q/U_0 = 4$, 5 and 6 are shown in figures 2(*a*), 2(*b*) and 2(*c*), respectively. Two curves computed from our boundary-layer analysis using different values of δ/a are compared to the numerical simulation for $(Re,\ q/U_0) = (400,\ 4)$ in figure 2(*a*). The dashed line gives the results using $\delta/a = 0.17$, which is the boundary-layer thickness leading to the best fit for the lift and torque (see table 3). The dashed line correctly predicts that C_{D_p} decreases with increasing r, but the values of C_{D_p} are not close to the results of numerical simulation. The solid line gives the results using $\delta/a = 0.2$, which are much closer to the simulation results and correctly predict that C_{D_p} changes sign across the boundary layer. Figure 2(*b*) shows the comparison for the case $(Re,\ q/U_0) = (400,\ 5)$. Again, the dashed line gives the results from our boundary-layer analysis using the value of δ/a leading to the best fit for the lift and torque (see table 4). The solid line gives the results using a larger δ/a, which are in excellent agreement with the simulation results. Figure 2(*c*) shows the comparison for the case $(Re,\ q/U_0) = (400,\ 6)$. We plot only one curve from the boundary-layer analysis using $\delta/a = 0.14$. This value leads not only to the best fit for the lift and torque (see table 5), but also to excellent agreement for C_{D_p} in figure 2(*c*). This comparison demonstrates that our boundary-layer analysis can be

Solution	Re	q/U_0	α	C_{D_p}	C_{D_f}	C_D	C_{L_p}	C_{L_f}	C_L	C_T
Numerical simulation	200	4	–	0.728	−0.604	0.124	16.961	0.621	17.582	0.453
This work	200	4	0.863	−0.188	−0.754	−0.942	17.907	0.729	18.636	0.476
Glauert's solution	200	4	0.625	0	−0.795	−0.795	20.102	0.795	20.897	0.215
Moore's solution	200	4	–	–	–	–	–	–	–	0.408
Numerical simulation	200	5	–	0.824	−0.835	−0.0107	26.183	0.846	27.029	0.514
This work	200	5	0.575	−0.0296	−0.893	−0.922	25.870	0.883	26.752	0.507
Glauert's solution	200	5	0.457	0	−0.929	−0.929	27.483	0.929	28.412	0.195
Moore's solution	200	5	–	–	–	–	–	–	–	0.440
Numerical simulation	400	4	–	0.534	−0.451	−0.0836	17.609	0.447	18.057	0.275
This work	400	4	0.779	−0.258	−0.530	−0.788	18.094	0.509	18.603	0.277
Glauert's solution	400	4	0.625	0	−0.562	−0.562	20.102	0.562	20.664	0.152
Moore's solution	400	4	–	–	–	–	–	–	–	0.237
Numerical simulation	400	5	–	0.591	−0.601	−0.010	26.415	0.597	27.011	0.297
This work	400	5	0.548	0.112	−0.617	−0.504	25.420	0.618	26.038	0.297
Glauert's solution	400	5	0.457	0	−0.657	−0.657	27.483	0.657	28.140	0.138
Moore's solution	400	5	–	–	–	–	–	–	–	0.246
Numerical simulation	400	6	–	0.668	−0.681	−0.0136	33.09	0.682	33.77	0.316
This work	400	6	0.432	0.676	−0.686	−0.0105	32.31	0.714	33.03	0.325
Glauert's solution	400	6	0.365	0	−0.736	−0.736	34.46	0.736	35.20	0.126
Moore's solution	400	6	–	–	–	–	–	–	–	0.263
Numerical simulation	1000	3	–	0.213	−0.197	0.0155	10.41	0.192	10.60	0.118
This work	1000	3	1.17	−0.755	−0.273	−1.028	11.08	0.232	11.31	0.130
Glauert's solution	1000	3	1.06	0	−0.273	−0.273	11.81	0.273	12.08	0.108
Moore's solution	1000	3	–	–	–	–	–	–	–	0.131

TABLE 7. The comparison of the solution in this work, using $\delta/a = 0.25$, 0.21, 0.17, 0.15, 0.14 and 0.12 for $(Re, q/U_0) = (200, 4)$, (200, 5), (400, 4), (400, 5), (400, 6) and (1000, 3) respectively, with the simulation results and Glauert's and Moore's solutions. Note that in our problem, the drag on the cylinder is negative if it is in the uniform flow direction; the drag is positive if it is opposite to the uniform flow direction (see figure 1). We call the readers' attention to the fact that $\alpha > 1$ in our solution and in Glauert's solution when $(Re, q/U_0) = (1000, 3)$; the solutions are not expected to converge to the true results.

used to compute the variation of the pressure drag across the boundary layer and the agreement with the numerical simulation becomes better as q/U_0 increases.

The functions $C_{L_p}(r)$ for three cases, $Re = 400$ and $q/U_0 = 4$, 5 and 6 are shown in figure 3. In all the three cases, C_{L_p} computed from our boundary-layer analysis are in excellent agreement with the numerical simulation. The theory correctly predicts the variation of C_{L_p} with r inside the boundary layer, which is a significant improvement on the irrotational theory and the classical boundary-layer theory of Prandtl. The lift force $L = \rho U_0 \Gamma$ from the irrotational theory is a constant at any $r \geqslant a$ because the circulation is a constant. In the classical boundary-layer theory, the pressure is a constant across the boundary layer and the variation of $C_{L_p}(r)$ shown in figure 3 cannot be obtained.

6. Higher-order boundary-layer theory

Glauert's analysis is a first-order boundary-layer approximation for the flow past a rotating cylinder. Our analysis here is intended to be an improvement of his boundary-layer solution. Another possible way to improve Glauert's solution is the higher-order

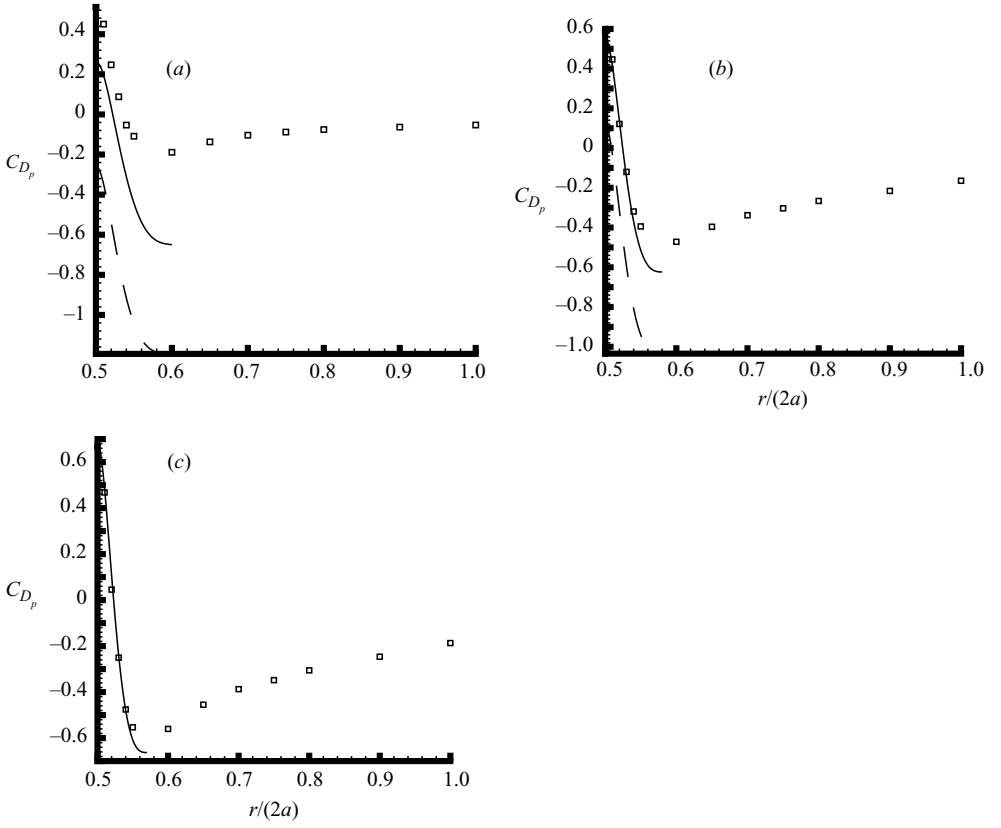

FIGURE 2. Comparison of the coefficient for the pressure drag C_{D_p} as a function of the radial position. (*a*) $Re = 400$, $q/U_0 = 4$. Our boundary-layer analysis: dashed line, using $\delta/a = 0.17$; solid line, using $\delta/a = 0.2$. The results of numerical simulation: □. (*b*) $Re = 400$, $q/U_0 = 5$. Our boundary-layer analysis: dashed line, using $\delta/a = 0.15$; solid line, using $\delta/a = 0.16$. The results of numerical simulation: □. (*c*) $Re = 400$, $q/U_0 = 6$. Our boundary-layer analysis using $\delta/a = 0.14$: solid line. The results of numerical simulation: □. C_{D_p} from our boundary-layer analysis can be computed only inside the boundary layer: $a \leqslant r \leqslant a + \delta$; C_{D_p} from numerical simulation is plotted up to $r = 2a$.

boundary layer theory based on the method of matched asymptotic expansions (Lagerstrom & Cole 1955; Van Dyke 1962*a*, 1969; Maslen 1963). We discuss the differences between our approach and the higher-order boundary-layer theory.

The basic idea of the higher-order boundary-layer theory is to construct outer and inner asymptotic expansions, by iterating the Navier–Stokes equations about the outer solution and about the boundary-layer solution, respectively, and to match the two expansions in their overlap regions of validity. Tani (1977) remarked, 'Higher approximations have thus been found only for flows without separation. In such cases the first term of the outer expansion is the inviscid irrotational flow, from which the first term of the inner expansion is determined by Prandtl's approximation. The second term of the outer expansion is the irrotational flow due to an apparent source distribution representing the displacement effect of Prandtl's boundary layer. This then determines a correction to the boundary-layer solution, yielding the second term of the inner expansion.' The second-order corrections are terms proportional to $1/\sqrt{Re}$ and the third-order terms are proportional to $1/Re$. Since the viscous term in the

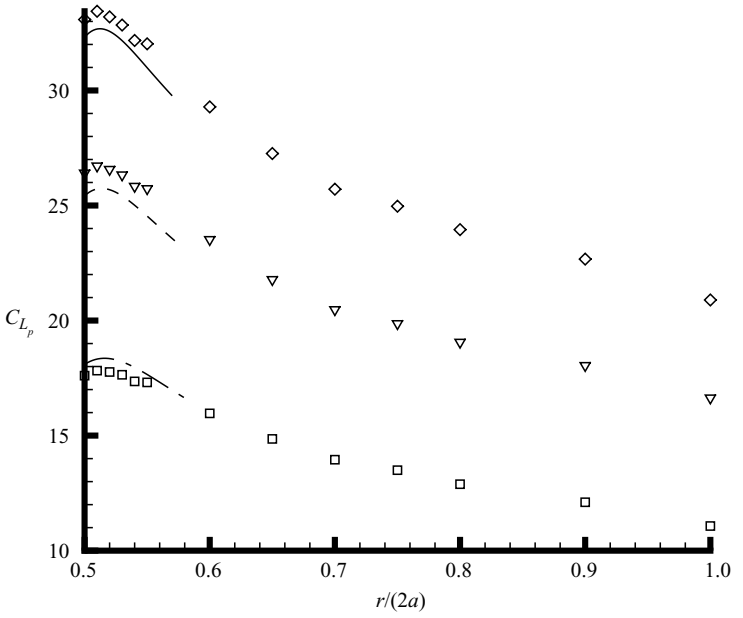

FIGURE 3. Comparison of the coefficient for the pressure lift C_{L_p} as a function of the radial position for $Re = 400$. Our boundary-layer analysis: dash-dotted line, $q/U_0 = 4$; dashed line, $q/U_0 = 5$; solid line, $q/U_0 = 6$. Numerical simulation: □, $q/U_0 = 4$; ∇, $q/U_0 = 5$; ◇, – $q/U_0 = 6$. C_{L_p} from our boundary-layer analysis can be computed only inside the boundary layer: $a \leqslant r \leqslant a + \delta$; C_{L_p} from numerical simulation is plotted up to $r = 2a$.

Navier–Stokes equations for the outer flow is of the order of $1/Re$, the higher-order theory must compute the third-order corrections to account for the viscous effects of the outer flow. Van Dyke (1969) remarked, 'Definite results in the literature are restricted mostly to laminar boundary layer, to steady motion, to plane or axisymmetric flows, and to the second approximation.' We are not aware of any third-order corrections in the literature. For incompressible fluids, the first- and second-order terms for the outer expansion are irrotational (Panton 1984; Tani 1977); it is not clear whether the third-order term is irrotational or not. Suppose the outer flow is irrotational at all orders and the fluid is incompressible, the viscous term $\mu\nabla^2\boldsymbol{u}$ disappears identically, which indicates that the viscous effects of the outer potential flow do not enter the higher-order boundary-layer theory if only velocity is matched but stress is not considered. Suppose the third-order term for the outer flow is rotational, the viscous term is then proportional to $1/Re$, which should give viscous effects to the inner solution at the third order.

Our new approach to boundary-layer flow is different from the higher-order boundary-layer theory and is not based on the method of matched asymptotic expansions. The matching conditions at the outer edge of the boundary layer are for the velocity in higher-order boundary-layer theory; shear stress has not been considered. We enforce the continuity of the shear stress at the outer edge of the boundary layer. Because we are considering a single fluid, the viscosity is the same inside and outside the boundary layer. The continuity of the shear stress is equivalent to continuity of velocity gradients. Since the velocity gradients for the outer flow are of order 1, our approach is not the same as the third-order corrections of the higher-order boundary theory.

Glauert's analysis is a first-order boundary-layer approximation. He ignored the irrotational rotary flow component of the flow in the boundary layer, which is

justifiable because the irrotational rotary flow is a second-order effect in the boundary layer. The torque coefficient by Glauert is of the order of $1/\sqrt{Re}$, and the torque coefficient in a purely irrotational rotary flow (without forward flow) is of the order of $1/Re$. However, numerical simulation shows that the higher-order correction is not negligible in this case. When $Re = 400$ and $q/U_0 = 6$, the torque coefficient by Glauert is only 40 % of the result of numerical simulation. It is conceivable that higher-order boundary-layer theory using the method of matched asymptotic expansions can be applied to this problem and yield corrections for Glauert's solution; but this has not been done. Our analysis is compared to the numerical simulation and good to excellent agreement is observed. Admittedly, the outer flow in our analysis is a first-order approximation and can be improved by higher-order corrections.

The pressure across the boundary layer can no longer be taken as a constant in higher-order theory. On a curved wall, centrifugal force produces a pressure gradient across the boundary layer, which is a second-order effect. Van Dyke (1969) inserted the irrotational surface speed with a correction due to the surface curvature into Bernoulli's equation for the external flow to compute the pressure at the outer edge of the boundary layer and it has no viscous terms. The pressure inside the boundary layer can be computed using this condition and the equation

$$\frac{\partial \overline{p}_2}{\partial n} = \kappa \overline{u}_1^2, \tag{83}$$

where $\overline{p}_2$ is the second-order correction for the pressure, n is normal to the surface, κ is the surface curvature and $\overline{u}_1$ is the first-order velocity from Prandtl's boundary-layer theory. Because $\overline{u}_1$ has viscous terms, the pressure at the wall computed from (83) should have viscous terms. However, in the applications of the higher-order theory to problems of leading edges and parabolas in uniform stream by Van Dyke (1962*b*, 1964), the second-order correction for the pressure was not computed; the drag is computed only using skin friction and the pressure is not considered.

In summary, the higher-order boundary-layer theory has not yet been applied to determine (1) the effect of the viscous dissipation of the outer irrotational flow; (2) the effect generated by a mismatch between the shear stress at the effective edge of the boundary layer and the irrotational shear stress there; (3) the drag and lift on the body due to normal stress associated with the viscous contribution to the pressure.

The numerical simulations of Padrino & Joseph (2006) show that the region in which the vortical effects are important is thick around the rotating cylinder. For example, the thickness of the vortical region determined using 1 % of the maximum vorticity magnitude criterion is 26 % of the cylinder radius for $Re = 400$ and $q/U_0 = 5$. The higher-order boundary-layer theory might encounter difficulty when treating such problems. Weinbaum *et al.* (1976) proposed an approximate method, which is not based on asymptotic analysis, to improve Prandtl's boundary-layer theory. They focused on flows with the Reynolds-number range $O(1) < Re < O(10^2)$, where the boundary layer is thick and a steady laminar wake is present. They remarked, 'It is not surprising in view of the large changes in effective body shape which the external inviscid flow must experience at these Reynolds numbers that a theory of successive approximation which is based on the potential flow past the original body shape will converge very slowly. This would appear to be the basic difficulty encountered in extending the results of second-order boundary-layer theory (Van Dyke 1962*a*, *b*) to flows with Reynolds numbers less than about 10^3.' The method of Weinbaum *et al.* is based on a pressure hypothesis which enables us to take account of the displacement interaction and centrifugal effects in thick boundary layers using conventional first-order boundary-layer

equations. Weinbaum *et al.* neglected the viscous term in the pressure which we have mentioned in the discussion of equation (83). They solved the momentum integral of the boundary-layer equations using the fourth-order Pohlhausen profile to obtain the displacement thickness. They treated the flows past parabolic and circular cylinders and obtained results in excellent agreement with numerical Navier–Stokes solutions. The method of Weinbaum *et al.* shares the common feature with ours that the boundary-layer thickness must be taken into account in the solution. However, like the higher-order boundary-layer theory, the method of Weinbaum *et al.* does not consider the shear stress discrepancy at the effective edge of the boundary layer, or the viscous contribution to the pressure.

7. Discussion and conclusion

The dependence of the lift on Re and q/U_0 is a key problem in the study of the flow past a rotating cylinder. Our work here and numerical simulations (Mittal & Kumar 2003; Padrino & Joseph 2006) show clearly that the lift force increases with increasing q/U_0; the major contribution to the lift is from the pressure, and the friction lift is much smaller than the pressure lift. The results of Padrino & Joseph (2006) show that the influence of the Reynolds number on the pressure lift is small; the friction lift seems to decrease with increasing Reynolds number (table 7). Glauert's prediction that the pressure lift is independent of Re, is a good approximation to the results of numerical simulation; our solution which considers the viscous effects on the pressure is in even better agreement with the results of numerical simulation. Kang, Choi & Lee (1999) simulated the flows with $Re = 40$, 60, 100 and 160 and q/U_0 between 0 and 2.5. The temporal-averaged values of pressure lift, pressure drag, friction lift and friction drag, computed after the flow becomes fully developed, were presented in their paper. They showed that the friction lift decreases with increasing Re and the pressure lift is nearly independent of Re. These results are consistent with Padrino & Joseph (2006) and our work, despite the fact that most of the flows studied by Kang *et al.* (1999) do not satisfy the assumptions that the separation is suppressed and steady-state solution exists.

The dependence of the drag on Re and q/U_0 is more complicated than the lift. Mittal & Kumar (2003) simulated the flows with $Re = 200$ and q/U_0 between 0 and 5; they presented the total drag coefficients C_D for the fully developed flows. The results show that when $q/U_0 < 1.91$, the flow is unsteady and the drag is oscillating; but the drag on the cylinder is always in the direction of the uniform flow. When $2 < q/U_0 < 4.34$ or $4.75 < q/U_0 < 5$, separation is suppressed and steady-state drag coefficients are obtained. The magnitude of C_D decreases with q/U_0 first, from about 0.3 at $q/U_0 = 2$ to about 0 at $q/U_0 = 3.25$. If q/U_0 is higher than 3.25, the magnitude of C_D is very close to zero; C_D could be slightly positive or negative. Kang *et al.* (1999) presented the temporal-averaged values for the total drag, pressure drag and friction drag. They showed that the magnitude of the total drag decreases with increasing q/U_0, but the total drag is in the same direction as the uniform flow for all the flows they studied. The magnitude of the pressure drag also decreases with increasing q/U_0; when $0 < q/U_0 < 2$, the pressure drag is in the same direction as the uniform flow, but when $q/U_0 = 2.5$, the pressure drag becomes opposite to the uniform flow. Similar results were obtained by Padrino & Joseph (2006), who showed that the pressure drag is opposite to the uniform flow for $q/U_0 = 3$, 4, 5, 6 and it is in competition with the friction drag, resulting in a total drag which is close to zero (see tables 1–6). The reason why the pressure drag becomes opposite to the uniform flow is not understood.

The pressure drag is a viscous effect. It cannot be studied using the classical boundary-layer theory, in which the irrotational pressure is imposed on the solid. Our boundary-layer solution is able to give a pressure drag. The agreement between this pressure drag and the result of numerical simulation depends on the choice of the boundary-layer thickness in our calculation. When q/U_0 is not high enough ($q/U_0 = 4$ or 5), it seems that the value of δ/a which gives rise to a good agreement for the pressure drag is larger than the value of δ/a which leads to good agreements for the lift and torque (see tables 1–4 and figure 2). In the case $(Re, q/U_0) = (400, 6)$, we can find a single value of δ/a which leads to good agreement for all the three quantities lift, torque and drag (see table 5), demonstrating that the agreement between our solution and numerical simulation becomes better as q/U_0 increases.

We have presented a comprehensive comparison for the drag, lift and torque on the cylinder given by our solution, by Glauert's (1957) solution, by Moore's solution (1957) and by the numerical simulation (Padrino & Joseph 2006). The comparison demonstrates that Moore's torque is relatively close to the simulation results, and Glauert's solution gives reasonable approximations for the friction drag and lift, but poor approximation for the torque. Our solution gives the best approximation to the numerical simulation when the value of δ/a is chosen to fit the numerical data. We also compared the profiles of the pressure drag and lift inside the boundary layer given by our solution and given by numerical simulation. The agreement of the lift profile is good (figure 3); the agreement of the drag profile is less good for small values of q/U_0, but improves as q/U_0 increases (figure 2). Such profiles are not available in Prandtl's boundary-layer theory, in which the pressure is equal to the irrotational pressure throughout the boundary layer.

The accuracy of our solution is affected mainly by the values of $\alpha = 2U_0/q$ and δ/a. Since we only carried out the calculation up to terms quadratic in α, the solution can be accurate only when α is very small. From table 7, we can see that the smallest value of α corresponds to $(Re, q/U_0) = (400, 6)$; other values of α in our work are all larger than 0.5. This is one of the reasons why the agreement between our solution and the numerical simulation is best for the case $(Re, q/U_0) = (400, 6)$. The boundary-layer thickness depends on the azimuthal angle θ, but we are not able to determine this dependence. We assume that δ is a constant for given Re and q/U_0 and the value of δ/a used in our calculation may be viewed as an average boundary-layer thickness. Padrino & Joseph (2006) determined δ/a at different azimuthal angle using the criterion that the vorticity magnitude at $r = a + \delta$ is approximately 1 % of the maximum magnitude of the vorticity field. They plotted δ/a as a function of θ (figure 6 in Padrino & Joseph 2006). The figure shows that the deviation of δ/a from its average is large when Re or q/U_0 is small, and the deviation is small when Re and q/U_0 are large. This result may explain why the agreement between our solution and numerical simulation becomes better when Re and q/U_0 increase.

The problem confronted in this work is that there is no precise end to the boundary layer, although most of the vorticity is confined to a region near to the spinning cylinder when the ratio of cylinder rotating speed to uniform stream speed q/U_0 is large. We have addressed this problem using the idea of an effective boundary-layer thickness, which is determined by matching with the results of numerical simulation. The thickness depends on the choice of quantities for the matching. We are able to match lift, drag and torque from our boundary-layer analysis for large values of q/U_0 and Re. In the companion paper, Wang & Joseph (2006), an effective boundary layer thickness was found which gave rise to reasonable matching for the pressure lift and torque on the cylinder computed from a simple modification of Glauert's

solution (1957), and for the pressure drag computed from the method of viscous correction of viscous potential flow (VCVPF). The values of the effective thickness in Wang & Joseph (2006) are about 1/2 or 1/3 of the values in this work. A method to determine the boundary-layer thickness without the aid of numerical simulation should be developed.

This work was supported in part by the NSF under grants from Chemical Transport Systems.

REFERENCES

Ece, M. C., Walker, J. D. A. & Doligalski, T. L. 1984 The boundary layer on an impulsively started rotating and translating cylinder. *Phys. Fluids* **27**, 1077–1089.

Glauert, M. B. 1957 The flow past a rapidly rotating circular cylinder. *Proc. R. Soc. Lond.* A **242**, 108–115.

Joseph, D. D. & Wang, J. 2004 The dissipation approximation and viscous potential flow. *J. Fluid Mech.* **505**, 365–377.

Kang, S., Choi, H. & Lee, S. 1999 Laminar flow past a rotating circular cylinder. *Phys. Fluids.* **11**, 3312–3321.

Kang, I. S. & Leal, L. G. 1988 The drag coefficient for a spherical bubble in a uniform streaming flow. *Phys. Fluids* **31**, 233–237.

Lagerstrom, P. A. & Cole, J. D. 1955 Examples illustrating expansion procedures for the Navier–Stokes equations. *J. Rat. Mech. Anal.* **4**, 817–882.

Levich, V. G. 1949 The motion of bubbles at high Reynolds numbers. *Zh. Eksperim. Teor. Fiz.* **19**, 18.

Lighthill, M. J. 1963 In *Laminar Boundary Layers* (ed. L. Rosenhead), chap. 2. Oxford University Press.

Maslen, S. H. 1963 Second-order effects in laminar boundary layers. *AIAA J.* **1**, 33–40.

Mittal, S. & Kumar, B. 2003 Flow past a rotating cylinder. *J. Fluid Mech.* **476**, 303–334.

Moore, D. W. 1957 The flow past a rapidly rotating circular cylinder in a uniform stream. *J. Fluid Mech.* **2**, 541–550.

Moore, D. W. 1959 The rise of a gas bubble in a viscous liquid. *J. Fluid Mech.* **6**, 113–130.

Moore, D. W. 1963 The boundary layer on a spherical gas bubble. *J. Fluid Mech.* **16**, 161–176.

Padrino, J. C. & Joseph, D. D. 2006 Numerical study of the steady state uniform flow past a rotating cylinder. *J. Fluid Mech.* **557**, 191–223.

Panton, R. L. 1984 *Incompressible Flow*. Wiley-Interscience.

Prandtl, L. & Tietjens, O. G. 1936 *Applied Hydro-and Aero-mechanics*. McGraw–Hill.

Pretsch, J. 1938 Zur theoretischen berechnung des profilwiderstandes. *Jahrb. d. dt. Luftfahrtforschung* **1**, 61. Engl. transl. *NACA TM* 1009 (1942).

Schlichting, H. 1960 *Boundary layer theory* (trans. J. Kestin), 4th edn. McGraw–Hill.

Squire, H. B. & Young, A. D. 1938 The calculation of the profile drag of aerofoils. *ARC R & M* 1838.

Tani, I. 1977 History of boundary-layer theory. *Annu. Rev. Fluid Mech.* **9**, 87–111.

Van Dyke, M. 1962*a* Higher approximations in boundary-layer theory. Part 1. General analysis. *J. Fluid Mech.* **14**, 161–177.

Van Dyke, M. 1962*b* Higher approximations in boundary-layer theory. Part 2. Application to leading edges. *J. Fluid Mech.* **14**, 481–495.

Van Dyke, M. 1964 Higher approximations in boundary-layer theory. Part 3. Parabola in uniform stream. *J. Fluid Mech.* **19**, 145–159.

Van Dyke, M. 1969 Higher-order boundary-layer theory. *Annu. Rev. Fluid Mech.* **1**, 265–292.

Wang, J. & Joseph, D. D. 2006 Pressure corrections for the effects of viscosity on the irrotational flow outside Prandtl's boundary layer. *J. Fluid Mech.* **557**, 145–165.

Weinbaum, S., Kolansky, M. S., Gluckman, M. J. & Pfeffer, R. 1976 An approximate theory for incompressible viscous flow past two-dimensional bluff bodies in the intermediate Reynolds number regime $O(1) < Re < O(10^2)$. *J. Fluid Mech.* **77**, 129–152.

Wood, W. W. 1957 Boundary layers whose streamlines are closed. *J. Fluid Mech.* **2**, 77–87.